SECURITY CLASSIFICATION OF THIS PAGE

AD-A237 128

REPORT DOCUMENTATIC

1a REPORT SECURITY CLASSIFICATION Unclassified	1b RESTRICTIVE MARKINGS
2a SECURITY CLASSIFICATION AUTHORITY	3 DISTRIBUTION/AVAILABILITY OF REPORT Unlimited
2b DECLASSIFICATION/DOWNGRADING SCHEDULE	
4 PERFORMING ORGANIZATION REPORT NUMBER(S) 5	5 MONITORING ORGANIZATION REPORT NUMBER(S)
6a NAME OF PERFORMING ORGANIZATION NIST — 6b OFFICE SYMBOL (If applicable)	7a NAME OF MONITORING ORGANIZATION ONR
6c ADDRESS (City, State, and ZIP Code) A329, Materials Building Gaithersburg, MD 20899	7b ADDRESS (City, State, and ZIP Code) Code 1131 800 N. Quincy Street Arlington, VA 22217-5000
8a NAME OF FUNDING/SPONSORING ORGANIZATION ONR — 8b OFFICE SYMBOL (If applicable)	9. PROCUREMENT INSTRUMENT IDENTIFICATION NUMBER N00014-90-F-0011
8c ADDRESS (City, State, and ZIP Code)	10 SOURCE OF FUNDING NUMBERS PROGRAM ELEMENT NO — PROJECT NO — TASK NO — WORK UNIT NO

11 TITLE (Include Security Classification)
Spatially and Spectrally Resolved Cathodoluminescence of Hot-Filament Chemical-Vapor-Deposited Diamond Particles

12 PERSONAL AUTHOR(S)
Lawrence H. Robins

13a. TYPE OF REPORT	13b. TIME COVERED	14 DATE OF REPORT (Year, Month, Day)	15. PAGE COUNT
Interim	FROM _____ TO _____	91-4-24	32

16 SUPPLEMENTARY NOTATION

17 COSATI CODES		
FIELD	GROUP	SUB-GROUP

18. SUBJECT TERMS (Continue on reverse if necessary and identify by block number)
This document has been approved for public release and sale: its distribution is unlimited.

19 ABSTRACT (Continue on reverse if necessary and identify by block number)

Spectrally resolved cathodoluminescence (CL) image and spatially resolved CL spectra were obtained from two specimens grown by hot-filament chemical vapor deposition. Each specimen consisted of a large number of unconnected diamond particles with cubo-octahedral and pseudo-five-fold twinned growth habits. The growth temperature was nominally 600° C for one specimen and 750° C for the other. In the 1.5-3.5 eV range, the spectra are composed of four defect and impurity related bands: there are three bands with zero-phonon lines at 1.68 eV, 2.156 eV, and 2.325 eV, and one broad band centered at 2.85 eV. A weak peak at 5.27 eV, due to exciton recombination, was also observed. Spectrally resolved images of the two most intense CL bands, at 2.156 eV and 2.85 eV, were obtained for several particles. In the low temperature specimen, bright regions in images of the 2.156 eV band are correlated with {111} facets; bright regions in images of the 2.85 eV band are correlated in some cases with the central regions of {100} facets, and in

20 DISTRIBUTION/AVAILABILITY OF ABSTRACT ☒ UNCLASSIFIED/UNLIMITED ☐ SAME AS RPT ☐ DTIC USERS	21 ABSTRACT SECURITY CLASSIFICATION Unclassified
22a NAME OF RESPONSIBLE INDIVIDUAL	22b TELEPHONE (Include Area Code) — 22c OFFICE SYMBOL

DD FORM 1473, 84 MAR — 83 APR edition may be used until exhausted. All other editions are obsolete.

SECURITY CLASSIFICATION OF THIS PAGE

Enclosure (1)

Block 19 Abstract (con't)

other cases with {111} facets. In the intermediate-temperature specimen, bright regions in the images of both bands are correlated with {100} facets. A model of competing recombination at different types of CL centers and non-radiative centers is proposed to facilitate the interpretation of the experimental results. For the low-temperature specimen, the model suggests that the 2.156 eV CL centers are located primarily in {111} growth sectors and the 2.85 eV CL centers are distributed relatively uniformly; images of the two dominant CL bands are predicted to have a complementary relationship in particles where there are few competing non-radiative centers. For the intermediate-temperature specimens, the model suggests that non-radiative recombination is dominant, and that the CL image contrast arises primarily from a non-uniform distribution of non-radiative centers.

OFFICE OF NAVAL RESEARCH

Contract N00014-90-F-0011

R&T Project No. IRMT 025

TECHNICAL REPORT No. 5

Spatially and Spectrally Resolved Cathodoluminescence of Hot-Filament Chemical-Vapor-Deposited Diamond Particles

by

Lawrence H. Robins, Edward N. Farabaugh and Albert Feldman

submitted to

Journal of Materials Research

National Institute of Standards and Technology

Ceramics Division

Gaithersburg, MD 20899

April 24, 1991

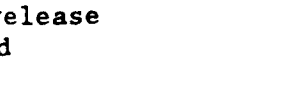

Spatially and spectrally resolved cathodoluminescence of hot-filament chemical-vapor-deposited diamond particles

Lawrence H. Robins, Edward N. Farabaugh, and Albert Feldman
National Institute of Standards and Technology, Gaithersburg, MD 20899

ABSTRACT

Spectrally resolved cathodoluminescence (CL) images and spatially resolved CL spectra were obtained from two specimens grown by hot-filament chemical vapor deposition. Each specimen consisted of a large number of unconnected diamond particles with cubo-octahedral and pseudo-five-fold twinned growth habits. The growth temperature was nominally 600° C for one specimen and 750° C for the other. In the 1.5-3.5 eV range, the spectra are composed of four defect and impurity related bands: there are three bands with zero-phonon lines at 1.68 eV, 2.156 eV, and 2.325 eV, and one broad band centered at 2.85 eV. A weak peak at 5.27 eV, due to exciton recombination, was also observed. Spectrally resolved images of the two most intense CL bands, at 2.156 eV and 2.85 eV, were obtained for several particles. In the low-temperature specimen, bright regions in images of the 2.156 eV band are correlated with {111} facets; bright regions in images of the 2.85 eV band are correlated in some cases with the central regions of {100} facets, and in other cases with {111} facets. In the intermediate-temperature specimen, bright regions in the images of both bands are correlated with {100} facets. A model of competing recombination at different types of CL centers and non-radiative centers is proposed to facilitate the interpretation of the experimental results. For the low-temperature specimen, the model suggests that the 2.156 eV CL centers are located primarily in {111} growth sectors and

the 2.85 eV CL centers are distributed relatively uniformly; images of the two dominant CL bands are predicted to have a complementary relationship in particles where there are few competing non-radiative centers. For the intermediate-temperature specimens, the model suggests that non-radiative recombination is dominant, and that the CL image contrast arises primarily from a non-uniform distribution of non-radiative centers.

I. INTRODUCTION

Natural and synthetic diamonds have been observed to contain many different types of optical centers that give rise to luminescence and optical absorption.[1,2] In diamond, the luminescence centers with known atomic structures are composed of point defects and impurity atoms;[1,2] some types of luminescence centers are thought to be associated with dislocations or other extended defects. Luminescence centers with inequivalent structures can in most cases be distinguished from each other by luminescence spectroscopy, which is a primary method of defect identification in diamond.

An electron beam with electron energy in the 1-50 keV range is known to be a relatively efficient luminescence excitation source for diamond.[3] Luminescence excited by an electron beam is referred to as cathodoluminescence (CL).[3] In the present work, a scanning electron microscope (SEM) is used as the CL excitation source. The imaging capability of the SEM allows the spatial distribution of the CL emission to be mapped with high spatial resolution.[4] Another advantage of utilizing the SEM is that the structural features revealed by CL imaging can be compared with the features revealed by secondary-electron emission or other imaging modes.

In previous publications, we presented CL spectra of synthetic diamond films and particles grown by hot-filament and microwave-plasma CVD.[5,6,7,8] We showed that only a few types of luminescence centers give rise to the CL spectra of these specimens. These centers, which were previously observed in natural or high-pressure synthetic diamond, are believed to be composed of vacancies, interstitials, dislocations, and the impurity atoms nitrogen and silicon. Other researchers have observed similar CL spectra in CVD diamond

specimens.[9,10,11] We also presented CL images of diamond particles obtained with the SEM.[5,6] The {100} facets of these particles were found to luminesce more intensely than the {111} facets. Other researchers have recorded CL images of CVD diamond films and particles, and found that the {100} facets were more luminescent than the {111} facets at most wavelengths.[12,13]

Here we present the results of a detailed study of two CVD diamond specimens by spatially and spectrally resolved CL in the SEM. Both of these specimens are composed of unconnected diamond particles on silicon substrates. The first specimen was grown at a low substrate temperature (relative to the temperature range for diamond deposition), nominally 600° C. In this specimen, unlike the previously examined specimens, the most intense CL band was found to be strongly correlated with {111} facets. In some particles from this specimen, the {111} facets were observed to luminesce more intensely than the {100} facets at all wavelengths; in other particles, the spectrally resolved CL images of the two dominant CL bands differed significantly from each other. The second specimen was grown at an intermediate substrate temperature (nominally 750° C). In this specimen, the total luminescence intensity was lower than in the first specimen, and the {100} facets were found to luminesce more intensely than the {111} facets at all wavelengths. These results are interpreted in terms of a model of the competing recombination of electron-hole pairs at different types of radiative (luminescent) and non-radiative recombination centers.

II. EXPERIMENTAL PROCEDURE

The diamond specimens were grown in a tube-furnace hot-filament CVD

reactor; the design of this reactor has been described previously.[14] The following conditions were used for both depositions: gas mixture, 0.5% methane and 99.5% hydrogen; feed gas mass-flow rate, 52 standard cm^3/min; pressure, $5x10^3$ Pa; filament temperature, 1800° C; deposition time, 115 hours. The nominal substrate temperature was 600° C for one deposition and 750° C for the other. These temperatures correspond respectively to the lower limit and to the middle of the diamond growth range for the particular hot-filament deposition system used here. Because of radiative heating by the filament, the actual temperature of the top surface of the substrate is probably higher than the nominal temperature, which is measured on the substrate holder beneath the substrate. Both specimens were grown on (100) oriented silicon substrates. Because a low nucleation density of diamond particles on the substrates was required for these depositions, the substrates were not prepared by polishing with diamond paste or powder. Such substrate preparation is commonly used to increase the diamond nucleation density when the growth of dense polycrystalline films is desired.

The experimental apparatus for CL imaging and spectroscopy is based on a conventional scanning electron microscope, and has been described previously.[5] The electron-beam voltage for the CL measurements was 20 kV, and the electron-beam current was $\sim 10^{-8}$ A. CL images were recorded by a red-sensitive photomultiplier tube (PMT) connected to a video imaging system; the wavelength range of the PMT is 200 to 850 nm. The spatial resolution of these images was ~0.5 μm. Spectrally resolved CL images were obtained by inserting optical bandpass filters, with a full width at half maximum (FWHM) of 40 nm, in the optical path before the PMT. CL spectra were measured by a 0.34 meter grating monochromator and an optical multichannel analyzer that utilizes an

intensified photodiode detector array. The spectral range covered with this monochromator and detector array was 200 to 900 nm, and the wavelength resolution was ~0.7 nm. Spectra were obtained from areas as small as 2x2 μm.

III. EXPERIMENTAL RESULTS

A. Spectrally resolved cathodoluminescence images

Spectrally resolved CL images and secondary-electron (SE) images of seven particles from the low-temperature specimen are shown in Figs. 1(a)-1(g). We will designate the particles shown in Figs. 1(a)-1(g) as particles 1 to 7 respectively. Each particle is represented by two spectrally resolved CL images and one SE image. The CL images represent the emission from two wavelength ranges selected by optical bandpass filters, both with bandwidths of 40 nm, one centered at 600 nm (2.07 eV) and the other centered at 450 nm (2.76 eV). For conciseness, we will refer to these as the 600 nm CL images and 450 nm CL images, respectively. The selected wavelength ranges correspond approximately to the two dominant spectral components of the CL.

The surface morphologies are imaged sharply in the SE images, but are blurred in the CL images because of electron beam penetration and spreading. According to semi-empirical models of electron scattering in solids,[4,15] the maximum penetration range of 20 keV electrons in diamond, R_e, is ~2.8 μm. The depth of maximum energy dissipation,[15] which should correspond to the maximum excitation of CL, is estimated to be $0.41R_e$ to $0.56R_e$ for carbon, or ~1.4 μm for 20 keV electrons in diamond. Particles 1-7 are ~20 μm in diameter; the CL

thus arises from the near-surface regions of these particles rather than from their entire depths. For comparison, we recorded CL images of some particles with 10 keV excitation, which should correspond to a range R_e of ~0.9 μm; the latter images did not differ significantly from those recorded at 20 keV.

We wish to describe how the CL images of particles 1-7 are related to the crystal growth habits. It is thus useful to establish a terminology for the description of the crystal growth habits. Particles 1 to 5 have approximately cubo-octahedral shapes. A perfect cubo-octahedron is made up of square {100} facets and triangular {111} facets, all sides being of equal length. In particles 1-5, the {100} facets are larger relative to the {111} facets than in a perfect cubo-octahedron, and thus tend to be octagonal rather than square in shape. The long sides of the {100} octagons form boundaries with {111} facets, and the short sides form boundaries with other {100} facets. Particles 6 and 7 have a pseudo-five-fold twinned morphology, commonly seen in CVD diamonds,[16] in which five adjacent {111} facets radiate from a common point. The lengths of the sides of the {100} and {111} facets in the pseudo-five-fold twinned particles are almost equal.

The edges between adjacent facets in particles (1)-(7) will be identified by the following scheme. Edges between {100} and {111} facets will be denoted type (a) edges; edges between pairs of {100} facets in the cubo-octahedral particles will be denoted type (b) edges; edges between pairs of {100} facets in the pseudo-five-fold twinned particles will be denoted type (c) edges; and edges between pairs of {111} facets in the pseudo-five-fold twinned particles will be denoted type (d) edges. Note that a perfect cubo-octahedron would contain only type (a) edges, and a perfect cube would contain only type (b) edges.

The 600 nm and 450 nm images of particles 1 and 2 are approximately complementary. For these particles, bright (or dark) regions in the 600 nm image are correlated with dark (or bright) regions in the 450 nm image. In the 600 nm images, the {111} facets appear brightest, and the centers of the {100} facets appear darkest. The dark regions in the 600 nm images tend to have cross-like shapes. This shape occurs when the dark region extends from the center to the four type (b) edges of a {100} facet. In the 450 nm images, {111} facets and regions of {100} facets near type (a) edges appear dark; the centers of {100} facets and type (b) edges appear bright. Especially in particle 2, the darkest regions in the 450 nm image appear to be correlated with the midpoints of type (a) edges, rather than with the centers of {111} facets.

For the other particles that we examined, the 600 nm images and 450 nm images are distinctly different, although not as close to complementary as they are for particles 1 and 2. The 450 nm CL images have a more variable form than the 600 nm images. This behavior is illustrated by the CL images of particles 3-5. In the 600 nm images, the bright regions are consistently correlated with {111} facets, or with the regions of {100} facets that lie near type (a) edges, and the dark regions are consistently correlated with the centers of {100} facets. Bright regions in the 450 nm images are in some cases correlated with the centers of {100} facets or with type (b) edges, as in particles 1 and 2. In particle 5, for example, the brightest region is correlated with a type (b) edge. In other cases, bright regions in the 450 nm images are correlated with {111} facets. The images of the pseudo-five-fold twinned particles, 6 and 7, show similar features. In the 600 nm images, bright regions are correlated with {111} facets; the darkest regions are

correlated with the centers of {100} facets; and secondary dark regions are correlated with type (d) edges. In the 450 nm images, the brightest regions are correlated with {111} facets, and secondary bright regions are correlated with the centers of {100} facets and with type (c) edges. Careful examination of the images of particles 3-7 shows that in each case where a particular {111} facet gives rise to bright regions in both the 600 nm image and the 450 nm image, the two images are readily distinguishable. In the 600 nm image, a region of relatively uniform brightness covers most of the {111} facet. In the 450 nm image, the bright region covers only part of the facet and has a non-uniform appearance.

Two spectrally resolved CL images and one SE image of a cubo-octahedral particle from the intermediate-temperature specimen, designated particle 8, are shown in Fig. 2. The morphology of particle 8 differs significantly from the morphologies of particles 1-7. The primary facets of particle 8 are covered with numerous secondary nucleation sites and growth steps. Examination of other particles from the intermediate-temperature specimen also reveals an abundance of secondary nucleation sites and growth steps. The formation of secondary nucleation sites, and of surface defects like growth steps, thus seems to be more probable at the intermediate growth temperature (nominally 750° C) than at the lower temperature (nominally 600° C).

Bright and dark regions occur in approximately the same locations in both the 600 nm CL image and the 450 nm CL image of particle 8. Comparison of the CL images with the SE image shows that variations in CL intensity within each primary facet are correlated with morphological features such as secondary nucleation sites. These morphological features are better resolved in the 450 nm CL image than in the 600 nm image. In both CL images, the

brightest regions are located within the {100} facets; the secondary bright regions within the {111} facets are seen to be correlated with secondary nucleation sites. These results are consistent with previous CL imaging results, which showed that the {100} facets of particles and polycrystalline films grown at intermediate temperature luminesce more intensely than the {111} facets.

The CL imaging results (Figs. 1 and 2) may be summarized as follows. In the low-temperature particles, bright regions in the 600 nm images are correlated with {111} facets or type (a) edges, and dark regions in the 600 nm images are correlated with the centers of {100} facets. The 450 nm images of the low-temperature particles vary considerably from particle to particle: the bright regions may be correlated with the centers of {100} facets, or with type (b) edges, or with irregularly shaped regions of {111} facets. In the intermediate-temperature particles, bright regions in both the 600 nm images and the 450 nm images are correlated with {100} facets or with regions of secondary nucleation inside the primary {111} facets.

One consistent feature of the CL images is that even the darkest (i.e., least luminescent) regions within the particles are brighter than the surrounding silicon substrate. This observation implies that there are no truly non-luminescent sectors within any of the diamond particles.

B. Spatially resolved cathodoluminescence spectra

CL spectra from selected regions of particles 2, 4, 6 and 8 are shown in Figs. 3(a) to 3(d) respectively. Two spectra are shown for each particle; one spectrum is taken from a selected region within a {100} facet, and the other

is taken from a selected region within a {111} facet. The selected regions, which are indicated by outlines in the SE images in Figs. 1 and 2, were chosen to coincide with bright or dark regions in the CL images.

Each of the four resolvable components of the CL spectra of these particles are apparent in the spectrum from the {100} facet of particle 6. This spectrum is replotted on an expanded intensity scale and the four resolvable components are labelled in Fig. 4. Three of the components give rise to sharp zero-phonon lines, at 1.68 eV, 2.156 eV, and 2.325 eV, together with lower-energy phonon sidebands. The fourth component is a broad, structureless band which peaks at ~2.85 eV. The phonon sidebands of the 2.156 eV line are particularly intense. These sidebands are due to coupling of the 2.156 eV center to 0.045 eV and 0.085 eV acoustic phonons and to the 0.165 eV longitudinal optical (LO) phonon;[17,18] features in the 2.156 eV spectrum associated with these phonons occur at approximately 2.11 eV, 2.07 eV, 1.99 eV, and 1.905 eV. (The fine structure in the 2.156 eV spectrum has been observed with better resolution in large gem-quality diamonds[17,18] than in the CVD diamond particles discussed in the present work.)

The photon energy ranges for the spectrally resolved CL images, selected by the 600 nm and 450 nm optical bandpass filters, are indicated by vertical dashed lines in Fig. 4. It can be seen that the CL selected by the 600 nm filter arises almost entirely from the 2.156 eV center, and the CL selected by the 450 nm filter arises almost entirely from the 2.85 eV center.

We have tentatively identified the structures of the luminescence centers that give rise to these four components, based on comparisons of our spectral results to results reported in the literature. The 1.68 eV line is attributed to a center that contains a silicon impurity atom.[19] The 2.156 eV

line, with its prominent phonon sidebands, is attributed to a nitrogen-vacancy center[17,18] (a center that contains both a nitrogen impurity atom and an atomic vacancy). The 2.325 eV line is tentatively attributed to another nitrogen-vacancy center[9] with a different atomic structure or electronic charge state than the 2.156 eV center. The broad 2.85 eV band is attributed to a dislocation-related center, which may be either a donor-acceptor pair or an intrinsic state associated with dislocations.[20]

It can be seen in Fig. 3 that the relative intensity of the 2.85 eV band is considerably higher from the {100} facets than from the {111} facets of the particles grown at low temperature. On the other hand, there is little difference between the spectra from the {100} facet and from the {111} facet of particle 8, grown at intermediate temperature. This variation in the shapes of the spectra can be quantified by calculating the ratio of the integrated intensity from 2.4 to 3.5 eV, which is dominated by the 2.85 eV band, to the total integrated intensity from 1.5 to 3.5 eV. The values of this ratio for particles 2, 3, 4, 6 and 8 are listed in Table I. (Spectra from particle 3 of the low-temperature specimen are similar to the spectra from particles 2, 4, and 6).

Other interesting features of these spectra are as follows. The 1.68 eV line attributed to the silicon impurity center is more prominent in the intermediate-temperature specimen (particle 8) than in the low-temperature specimen (particle 2, 4, and 6). The FWHM of the 2.156 eV line is larger in the intermediate-temperature specimen (0.030 eV for the {100} facet, too broad to be determined for the {111} facet) than in the low-temperature specimen (0.017-0.027 eV). The extra broadening of the 2.156 eV line in the intermediate-temperature specimen may arise from defect-defect interactions

with a higher density of defects than in the low-temperature specimen, or from larger residual stresses. The 2.325 eV zero-phonon line shows considerable variation in lineshape from one location to another in the low-temperature specimen, and even splits into two components in some locations. The splitting observed for the {111} facet of particle 4 [Fig. 3(b)] is displayed on an expanded scale in Fig. 5. If the 2.325 eV center possesses an orbitally degenerate electronic ground state, then the splitting of the zero-phonon line can be explained by the presence of an anisotropic residual stress. The origin of the anisotropic stress required to explain the observed splitting is not known.

CL spectra from particle 2 in the 5.0-5.6 eV photon energy range are plotted in Fig. 6. In diamond, the most intense exciton luminescence line, due to the recombination of an indirect exciton assisted by the emission of a transverse optical phonon, occurs at 5.27 eV.[11,21] This line is clearly visible above the noise in the spectrum from the {100} facet, but is distinctly weaker in the spectrum from the {111} facet. The asymmetric lineshape of the exciton line, broader on the high-energy than the low-energy side of the peak, is due to the thermal distribution of exciton energies. An empirical fit to the lineshape is also shown in Fig. 6. The FWHM of the fitted line, 0.066 eV, is somewhat larger than the value of 0.046 eV (or 1.8 kT at 300 K) expected if thermal broadening were the only source of line broadening. Like the zero-phonon lines of the defect centers, the exciton line may be broadened by the effects of disorder or residual stress.

IV. DISCUSSION

The image contrast in the spectrally resolved CL images (shown in Fig. 1) is thought to arise from an inhomogeneous spatial distribution of luminescence centers or competing non-radiative recombination centers. Here we present a recombination model that relates the observed image contrast to the spatial distributions of the various types of recombination centers. This model was presented in a different context in a previous publication[7], where it was used to interpret specimen-to-specimen variations in the intensity of the CL and of the PL excited by sub-band-gap photons.

The basic assumptions of the recombination model are as follows. The initial step for the excitation of CL in diamond is the creation of electron-hole pairs by the inelastic scattering of electrons from the primary electron beam. These free electron-hole pairs are then captured by or inelastically scattered from recombination centers, which undergo transitions from their ground states to excited electronic states. The recombination centers may be radiative (luminescent) or non-radiative. (We consider a center to be non-radiative if it does not give rise to observable luminescence in the 1.5-6 eV photon energy range). The various types of recombination centers thus compete with each other for excitation by the electron-hole pairs. It follows that the spatially resolved CL intensity from a particular type of center, which we designate as type (a), depends not only on the local concentration of type (a) centers, but also on the local concentrations of all other types of recombination centers. The intensity of the CL from the type (a) centers increases with increasing concentration of type (a) centers, but decreases with increasing concentrations of other types of centers.

If it is also assumed that only a small fraction of recombination centers of each type is excited out of the ground state, then the

concentrations of excited centers are directly proportional to the excitation intensity. The following equation for the intensity of the CL from the type (a) centers is then obtained.

$$I_{CL}(a) = [\eta_a B_a N_a \; / \; (\Sigma(B_i N_i) + \Sigma(b_j n_j))] \; G_{eh} \qquad (1)$$

where N_a is the concentration of luminescence centers of type (a); η_a is the internal luminescence quantum efficiency of the type (a) centers; N_i is the concentration of luminescence centers of type (i); n_j is the concentration of non-radiative recombination centers of type (j); B_a, B_i and b_j are the respective rates for the excitation of these centers by interactions with free electron-hole pairs; and G_{eh}, the electron-hole pair generation rate, is proportional to the intensity of the incident electron beam. [Note that the first summation in the denominator of Eq. (1) is over all types of luminescence centers, including type (a), and the second summation is over all types of non-radiative centers]. The quantities η_a, B_i, and b_j are assumed to be constants for each type of center, and the electron-hole generation rate G_{eh} is assumed to remain constant as the electron beam is scanned from one specimen location to another. The CL image contrast thus arises from the spatial variation of the concentrations N_a, N_i, and n_j.

We next consider some special cases of Eq. (1) which appear to be relevant to the present experimental results. Suppose first that there are two dominant types of luminescence centers, type (a) and type (b), and no competing non-radiative centers. Eq. (1) then assumes the form

$$I_{CL}(a) = [\eta_a B_a N_a \; / \; (B_a N_a + B_b N_b)] \; G_{eh} \qquad (2)$$

for type (a) centers, and the corresponding equation for the intensity of the CL from type (b) centers is:

$$I_{CL}(b) = [\eta_b B_b N_b \; / \; (B_a N_a + B_b N_b)] \; G_{eh} \qquad (3)$$

The sum of the CL intensities from the two types of centers, weighted by the inverse quantum efficiencies, is then equal to the constant G_{eh}.

$$I_{CL}(a)/\eta_a + I_{CL}(b)/\eta_b = G_{eh} \qquad (4a)$$

In this case, the image of the CL from the type (b) centers is complementary to the image of the type (a) CL; i.e., in a region of the specimen where the intensity of the type (a) CL is higher than its average value, the intensity of the type (b) CL is correspondingly lower:

$$I_{CL}(b) = G_{eh} - (\eta_b/\eta_a) \; I_{CL}(a) \qquad (4b)$$

The observation that the 600 nm and 450 nm CL images of particles 1 and 2, in Fig. 1, are approximately complementary is thus explained by a model in which the recombination is dominated by two types of CL centers. Recall that the 600 nm image is the image of the 2.156 eV CL centers; the 450 nm image is the image of the 2.85 eV centers; and these two types of centers are seen to dominate the CL spectra shown in Fig. 3. Note that, according to Eq. (4), the observation of complementary images does not indicate which type of center has a non-uniform spatial distribution. There are three possible cases: (1) the

2.156 eV centers are correlated with {111} growth sectors and the 2.85 eV centers are uniformly distributed; (2) the 2.156 eV centers are uniformly distributed and the 2.85 eV centers are correlated with {100} sectors; (3) the 2.156 eV centers are correlated with {111} growth sectors and the 2.85 eV centers are correlated with {100} sectors.

Consider next a specimen where there are two dominant types of CL centers, but non-radiative centers are also present. Eq. (1) can then be written as

$$I_{CL}(a) = [\eta_a B_a N_a \,/\, (B_a N_a + B_b N_b + \Sigma(b_j n_j))]\; G_{eh} \qquad (5)$$

for the type (a) centers, and a similar equation can be written for $I_{CL}(b)$. The analog of Eq. (4a) for the weighted sum of the CL intensities is then

$$I_{CL}(a)/\eta_a + I_{CL}(b)/\eta_b = G_{eh} \,/\, [1 + \Sigma(b_j n_j)/(B_a N_a + B_b N_b)] \qquad (6)$$

Because of the factor in brackets, the weighted sum of intensities is not constant in this system, and the two images are not necessarily complementary. This case fits the experimental results for particles 3-7, in Fig. 1, where there are two dominant CL bands but the CL images are not complementary. For these particles, the bright regions in the 600 nm images are consistently correlated with {111} facets, but the bright regions in the 450 nm images are correlated in some cases with the central regions of {100} facets and in other cases with irregularly shaped regions of {111} facets. All these observations are consistent with a simple model for the distribution of recombination centers in particles 1-7. According to this model, the 2.156 eV centers are

located primarily in {111} growth sectors; the 2.85 eV centers are relatively evenly distributed between {100} and {111} sectors; and non-radiative centers, if they are present in significant numbers, are located primarily in {100} sectors. Therefore, when there are few non-radiative centers, the 600 nm and 450 nm images have the complementary relationship observed for particles 1 and 2; on the other hand, when there is a high concentration of non-radiative centers in {100} sectors, the brightest regions in both images are correlated with {111} facets, as observed for particles 5-7.

Consider finally a specimen where the recombination is dominated by non-radiative centers, although CL centers are present in sufficient concentrations to be readily observable. Eq. (1) then has the form

$$I_{CL}(a) = [\eta_a B_a N_a \; / \; \Sigma(b_j n_j)] \; G_{eh} \qquad (7)$$

for the type (a) centers, and similar equations can be written for the intensity of the luminescence from type (b) centers, or centers of any other type. If the non-radiative centers are distributed uniformly throughout the specimen, then the spatial variation of $I_{CL}(a)$ is determined by the variation of N_a, as one might have naively expected before attempting to model the recombination processes. On the other hand, if the non-radiative centers have a non-uniform distribution, then the intensity of the CL from all types of centers will be higher (or lower) from locations where the concentration of non-radiative centers is lower (or higher). This case appears to fit the experimental results for the particles grown at intermediate temperature (particle 8, Fig. 2, and particles shown in our previous spectrally resolved CL study[5]). In the intermediate-temperature particles, bright regions in the

600 nm images and the 450 nm images are correlated with {100} facets and coincide almost perfectly with each other. The hypothesis that non-radiative recombination processes are dominant in the intermediate-temperature particles is supported by the observation that the total CL intensity is significantly lower for the intermediate-temperature particles [Fig. 3(d)] than for the low-temperature particles [Figs. 3(a)-3(c)]. Notice also that in particle 8 the ratio of the intensity of the 2.85 eV CL band to the intensity of the 2.156 eV band hardly varies between the {100} and {111} facets [Fig. 3(d) and Table I]. This result is consistent with a model in which the two dominant types of CL centers are distributed relatively uniformly; the CL image contrast in the intermediate-temperature particles thus arises from a non-uniform distribution of non-radiative recombination centers.

V. CONCLUSION

Spectrally resolved CL images and spatially resolved CL spectra were obtained from unconnected particles in two hot-filament CVD diamond specimens. The growth temperature was nominally 600° C for one specimen and 750° C for the other. The particles have cubo-octahedral or pseudo-five-fold twinned growth habits. The CL spectra of these particles contain four bands in the 1.5-3.5 eV range: three bands with zero-phonon lines at 1.68 eV, 2.156 eV, and 2.325 eV, and one broad band which peaks at 2.85 eV. A peak at 5.27 eV, which arises from exciton recombination, was observed in the spectrum of a particle from the low-temperature specimen. Spectrally resolved CL images of the two most intense CL bands, the 2.156 eV band and the 2.85 eV band, were obtained for several particles. In the low-temperature specimen, bright regions in

images of the 2.156 eV band (taken at 600 nm) are consistently correlated with {111} facets; bright regions in images of the 2.85 eV band (taken at 450 nm) are correlated in some cases with the central regions of {100} facets, and in other cases with sections of {111} facets. In the intermediate-temperature specimen, bright regions in both images are correlated with {100} facets, and the two images of the same particle are very similar to each other, as observed previously for another specimen grown at the same temperature.

To help interpret the experimental results, we propose a model in which different types of CL centers and non-radiative recombination centers compete for recombination of the initially excited electron-hole pairs. For the low-temperature specimen, comparison of the experimental results with the model suggests that the 2.156 eV CL centers are located primarily in {111} growth sectors and the 2.85 eV CL centers are distributed relatively uniformly. In particles where there are few competing non-radiative centers, images of the two dominant CL bands should then have a complementary relationship; in particles where there are many non-radiative centers in the {100} sectors, bright regions in both images should be correlated with {111} facets. For the intermediate-temperature specimens, the model suggests that non-radiative recombination is the dominant mode, and that the CL image contrast arises primarily from a non-uniform distribution of non-radiative centers, which are located primarily in {111} sectors in these specimens.

ACKNOWLEDGEMENTS

This work was supported in part by the Office of Naval Research.

REFERENCES

1. C. D. Clark, E. W. J. Mitchell and B. J. Parsons, in The Properties of Diamond, ed. by J. E. Field (Academic Press, London, 1979), p. 23
2. J. Walker, Rep. Prog. Phys. 42, 1605 (1979)
3. G. Davies, in The Properties of Diamond, ed. by J. E. Field (Academic Press, 1979), p. 165
4. B. G. Yacobi and D. B. Holt, J. Appl. Phys. 59, R1 (1986)
5. L. H. Robins, L. P. Cook, E. N. Farabaugh and A. Feldman, Phys. Rev. B 39, 13367 (1989)
6. L. H. Robins, L. P. Cook, E. N. Farabaugh and A. Feldman, in Diamond Optics II, ed. by A. Feldman and S. Holly, Proc. SPIE 1146, 166 (SPIE, Bellingham, WA, 1990)
7. L. H. Robins, E. N. Farabaugh, A. Feldman and L. P. Cook, accepted for publication in Phys. Rev. B (1991)
8. L. H. Robins, P. J. H. Tjossem, K. C. Smyth, P. Y. Barnes, E. N. Farabaugh and A. Feldman, accepted for publication in J. Appl. Phys. (1991)
9. V. S. Vavilov, A. A. Gippius, A. M. Zaitsev, B. V. Deryagin, B. V. Spitsyn and A. E. Aleksenko, Fiz. Tekh. Poluprovodn. 14, 1811 (1980) [Sov. Phys. Semicond. 14, 1078 (1980)]
10. A. T. Collins, M. Kamo and Y. Sato, J. Phys. D 22, 1402 (1989)
11. W. D. Partlow, J. Ruan, R. E. Witkowski, W. J. Choyke and D. S. Knight, J. Appl. Phys. 67, 7019 (1990)
12. H. Kawarada, K. Nishimura, T. Ito, J. Suzuki, K. Mar, Y. Yokota and A. Hiraki, Jpn. J. Appl. Phys. 27, L683 (1988)

13. H. Kawarada, Y. Yokota, Y. Mori, K. Nishimura and A. Hiraki. J. Appl. Phys. 67, 983 (1990)

14. E. N. Farabaugh, A. Feldman, L. H. Robins and E. S. Etz, in Diamond Optics, ed. by A. Feldman and S. Holly, Proc. SPIE 969, 24 (SPIE, Bellingham, WA, 1989)

15. K. Kanaya and S. Okayama, J. Phys. D: Appl. Phys. 5, 43 (1972)

16. J. Narayan, A. R. Srivatsa and K. V. Ravi, Appl. Phys. Lett. 54, 1659 (1989)

17. A. T. Collins, M. Stanley and G. S. Woods, J. Phys. D 20, 969 (1987)

18. A. T. Collins and S. C. Lawson, J. Phys. Condens. Matter 1, 6929 (1989)

19. A. M. Zaitsev, V. S. Vavilov and A. A. Gippius, Krat. Soob. Fiz. 10, 21 (1981) [Sov. Phys. - Leb. Inst. Rep. 10, 15 (1981)]

20. N. Yamamoto, J. C. H. Spence and D. Fathy, Phil. Mag. B 49, 609 (1984)

21. P. J. Dean, E. C. Lightowlers and D. R. Wight, Phys. Rev. 140, A352 (1965)

FIGURE CAPTIONS

1. Secondary-electron (SE) and spectrally resolved cathodoluminescence (CL) images of seven particles from diamond specimen grown by hot-filament CVD at low substrate temperature (nominally 600° C). The particles shown here are designated particles 1 to 7 respectively. Each particle is represented by three images: a SE image; a spectrally resolved CL image taken at a center wavelength of 600 nm; and a spectrally resolved CL image taken at a center wavelength of 450 nm. FWHM is 40 nm for both CL images. Outlined squares in SE images represent regions from which CL spectra (shown in Fig. 3, below) were taken. (a) Particle 1, cubo-octahedral habit. (b) Particle 2, cubo-octahedral habit. (c) Particle 3, cubo-octahedral habit. (d) Particle 4, cubo-octahedral habit. (e) Particle 5, cubo-octahedral habit. (f) Particle 6, pseudo-five-fold twinned habit. (g) Particle 7, pseudo-five-fold twinned habit.

2. Secondary-electron (SE) and spectrally resolved cathodoluminescence (CL) images of a particle from diamond specimen grown by hot-filament CVD at intermediate substrate temperature (nominally 750° C). This particle is designated particle 8. Three images are shown: a SE image; a spectrally resolved CL image taken at a center wavelength of 600 nm; and a spectrally resolved CL image taken at a center wavelength of 450 nm. Outlined squares in SE image represent regions from which CL spectra (shown in Fig. 3, below) were taken.

3. CL spectra from selected regions of particles 2, 4, 6 and 8. Two spectra are shown for each particle, one taken from a selected region of a {100} facet, the other taken from a selected region of a {111} facet. The selected regions are outlined in the SE images shown in Figs. 1 and 2. (a) Particle 2. (b) Particle 4. (c) Particle 6. (d) Particle 8.

4. CL spectrum from {100} facet of particle 6, plotted on expanded intensity scale. The four resolvable features of this spectrum are labelled. In order of increasing photon energy, these are attributed to a silicon impurity center (zero-phonon line at 1.68 eV, labelled "Si" in the figure); two types of nitrogen-vacancy centers (zero-phonon lines at 2.156 eV and 2.325 eV, labelled "N-V"); and a dislocation-related defect (broad band at 2.85 eV, labelled "DISLOC"). Vertical dashed lines indicate the photon energy ranges for the spectrally resolved CL images which are selected by 600 nm and 450 nm optical bandpass filters.

5. CL spectrum from {111} facet of particle 4, in vicinity of 2.325 eV zero-phonon line. Vertical and horizontal scales are expanded to best display the splitting of this line.

6. CL spectra from selected regions of particle 2 in 5.0 to 5.6 eV photon energy range. The luminescence line at 5.27 eV due to recombination of an indirect exciton, assisted by the emission of a transverse optical phonon, is clearly observable in the spectrum from the {100} facet. The dotted line represents an empirical fit to the exciton lineshape.

Table I. Ratio of the intensity of the 2.85 eV CL band (spectrally integrated CL from 2.4 eV to 3.5 eV) to the sum of intensities of the 1.68 eV, 2.156 eV, 2.325 eV, and 2.85 eV CL bands (spectrally integrated CL from 1.5 eV to 3.5 eV). range, for emission from selected areas of particles 2, 3, 4, 6, and 8. Particles 2, 3, 4, and 6 are from the specimen grown at low temperature (nominally 600° C); particle 8 is from the specimen grown at intermediate temperature (nominally 750° C). Particle 6 has a pseudo-five-fold twinned growth habit; the other particles have cubo-octahedral growth habits.

Particle	Facet	Intensity Ratio
2	{100}	0.334
2	{111}	0.022
3	{100}	0.340
3	{111}	0.028
4	{100}	0.340
4	{111}	0.033
6	{100}	0.114
6	{111}	0.035
8	{100}	0.334
8	{111}	0.329

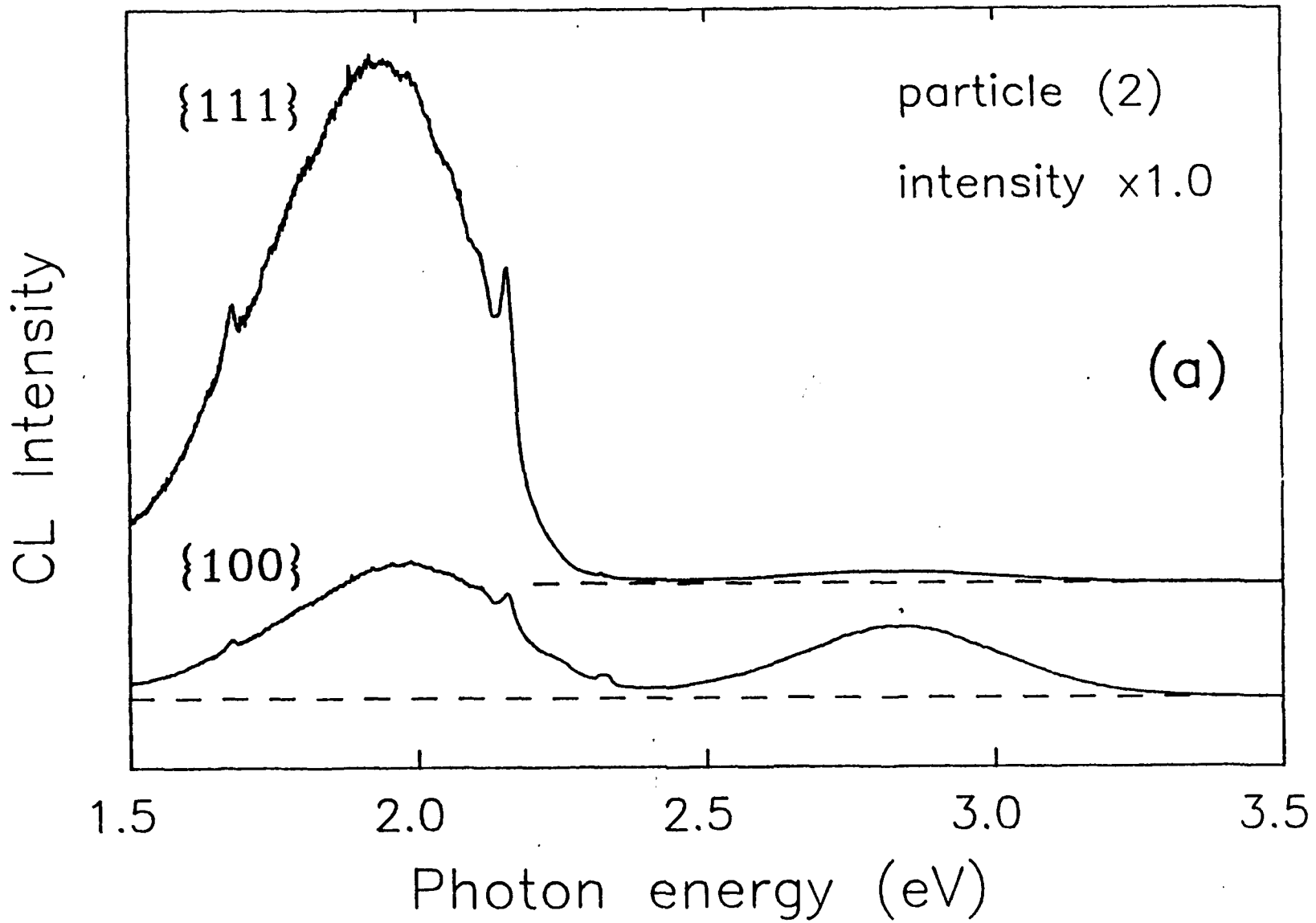
{111}
particle (2)
intensity x1.0
(a)
{100}
CL Intensity
1.5
2.0
2.5
3.0
3.5
Photon energy (eV)

FIG 3(a)

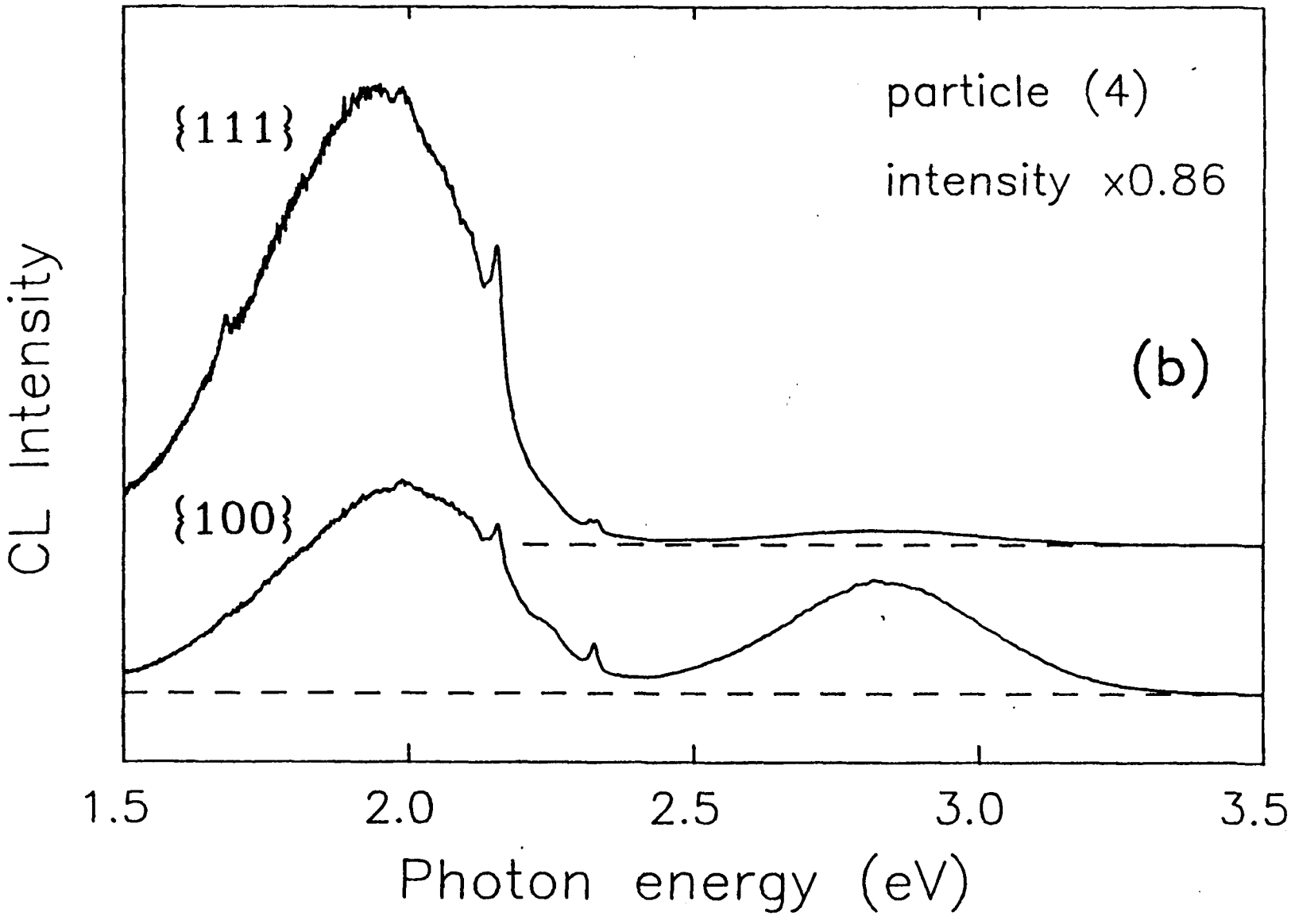
particle (4)
intensity x0.86
(b)
{111}
{100}
CL Intensity
1.5
2.0
2.5
3.0
3.5
Photon energy (eV)

FIG 3(b)

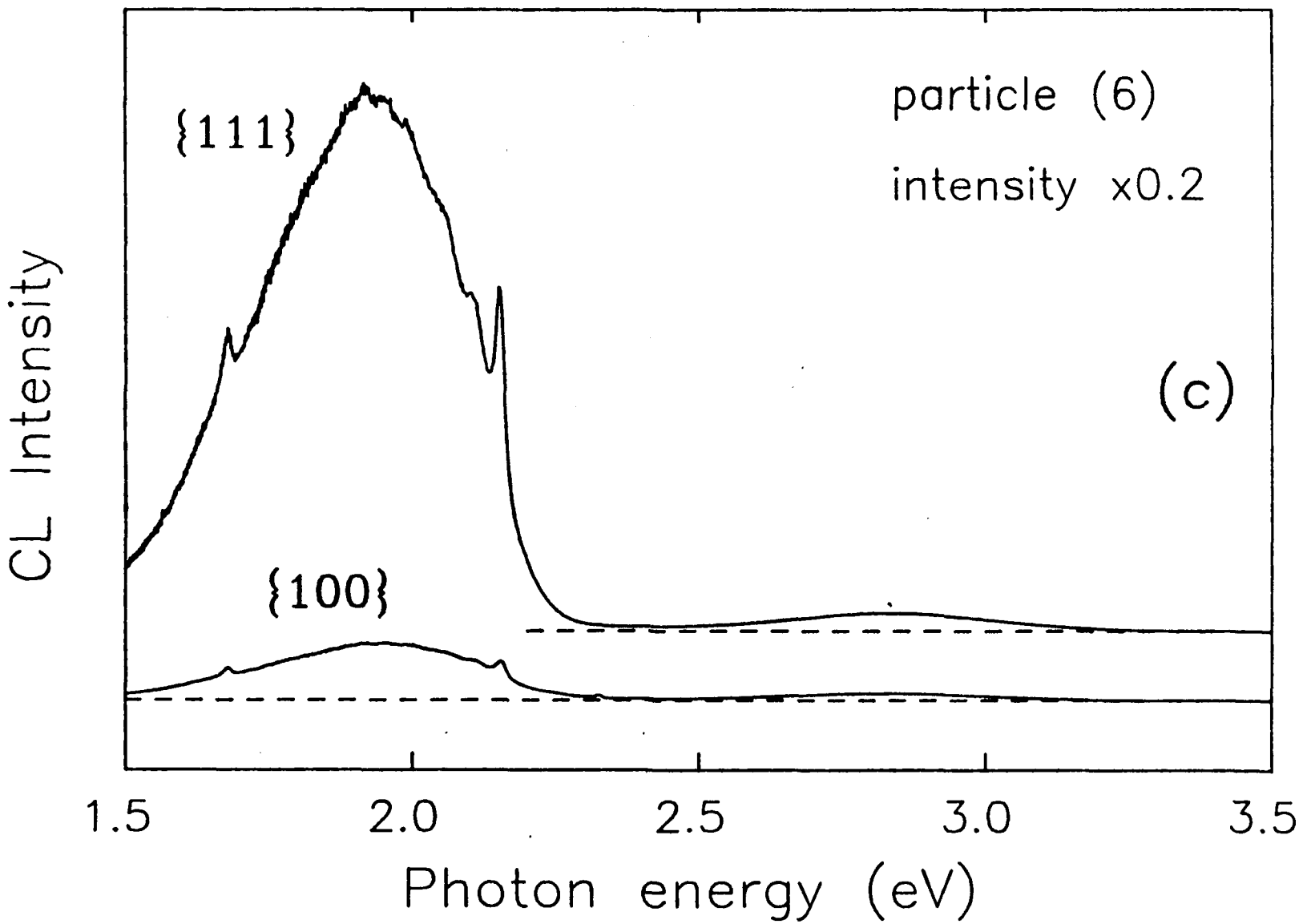
particle (6)
intensity x0.2
(c)
{111}
{100}
CL Intensity
1.5
2.0
2.5
3.0
3.5
Photon energy (eV)

FIG 3(c)

FIG 3(d)

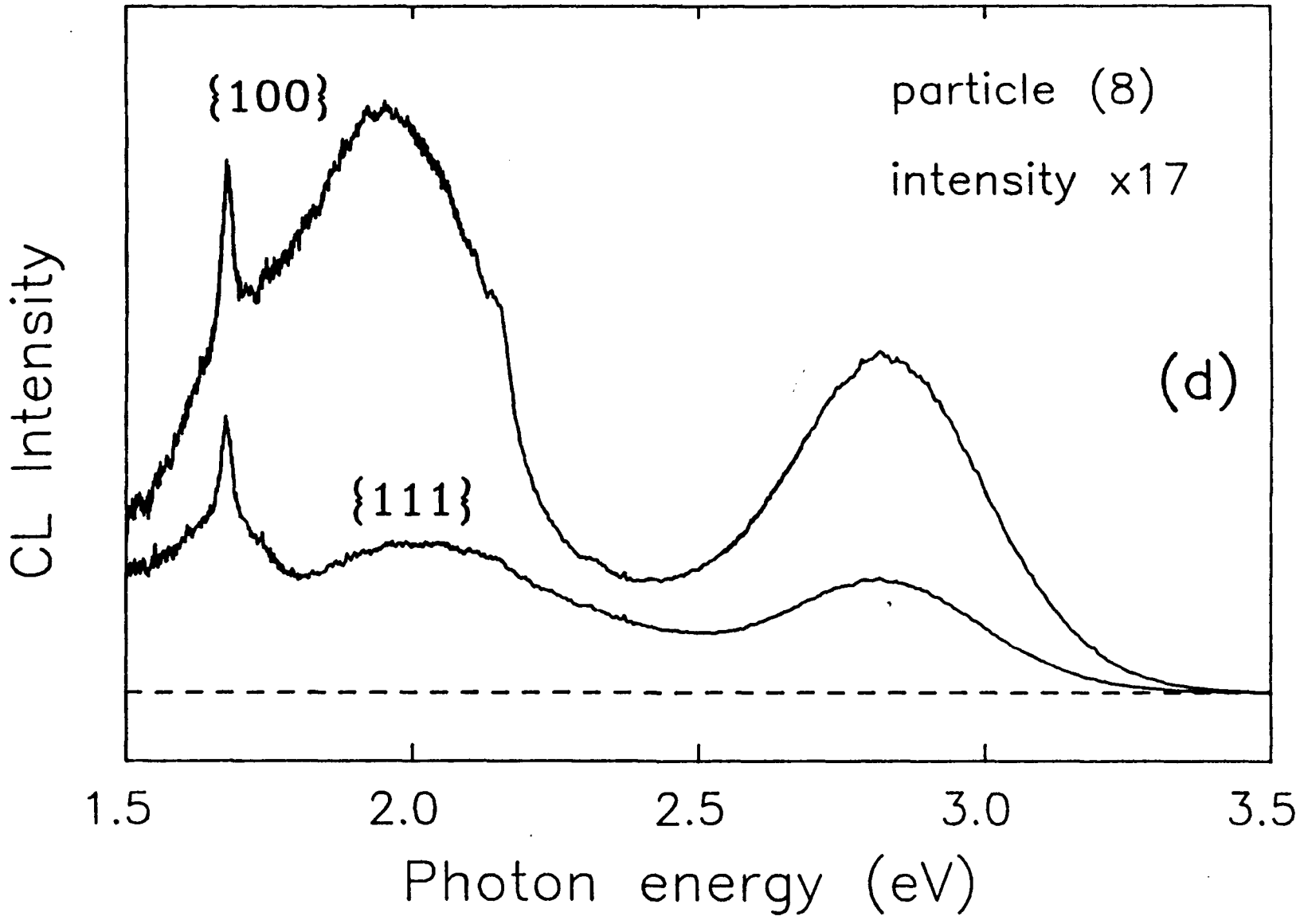
{100}
particle (8)
intensity x17
(d)
{111}
CL Intensity
1.5
2.0
2.5
3.0
3.5
Photon energy (eV)

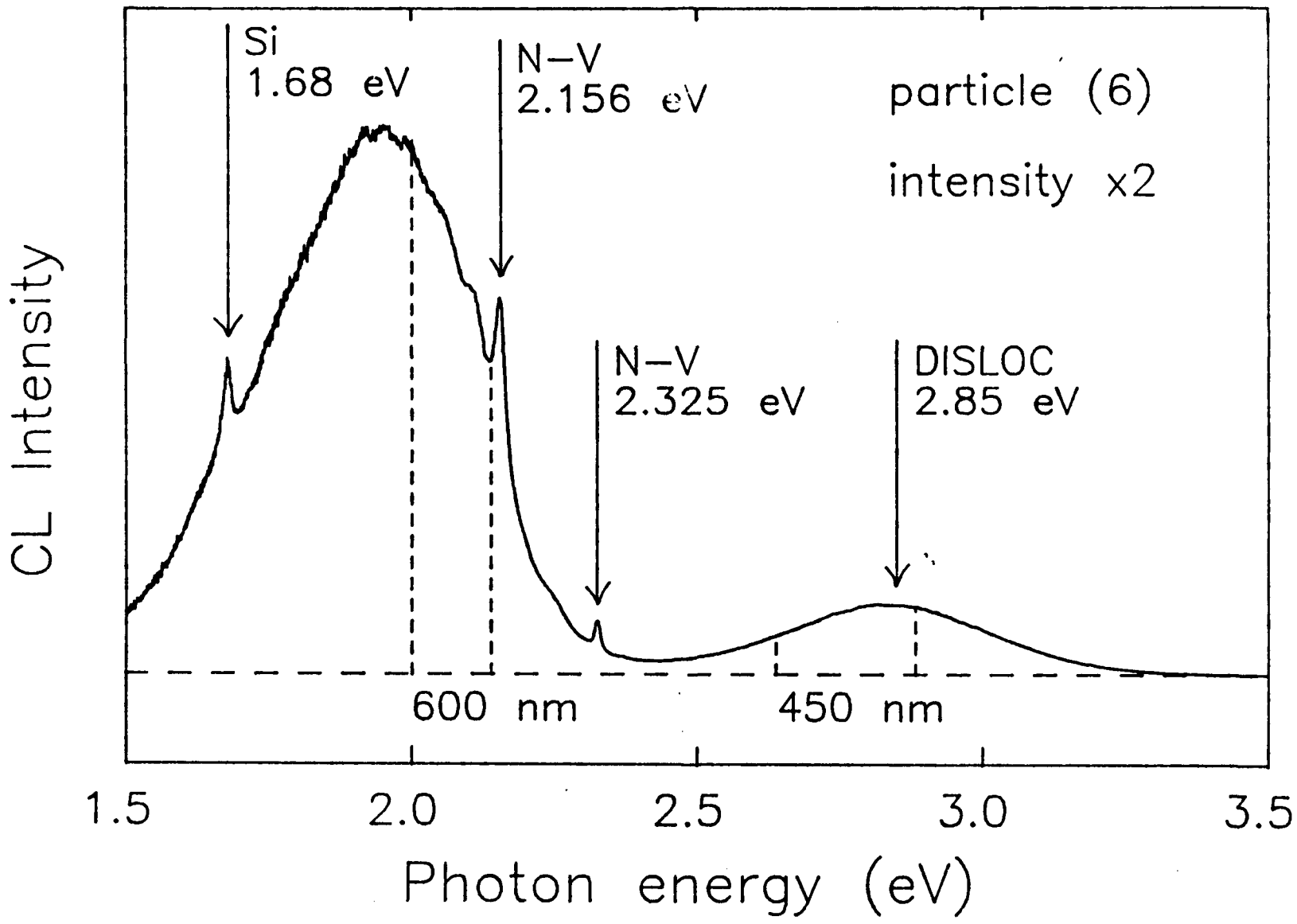
Si
1.68 eV
N–V
2.156 eV
particle (6)
intensity x2
N–V
2.325 eV
DISLOC
2.85 eV
600 nm
450 nm
CL Intensity
1.5
2.0
2.5
3.0
3.5
Photon energy (eV)

FIG 4

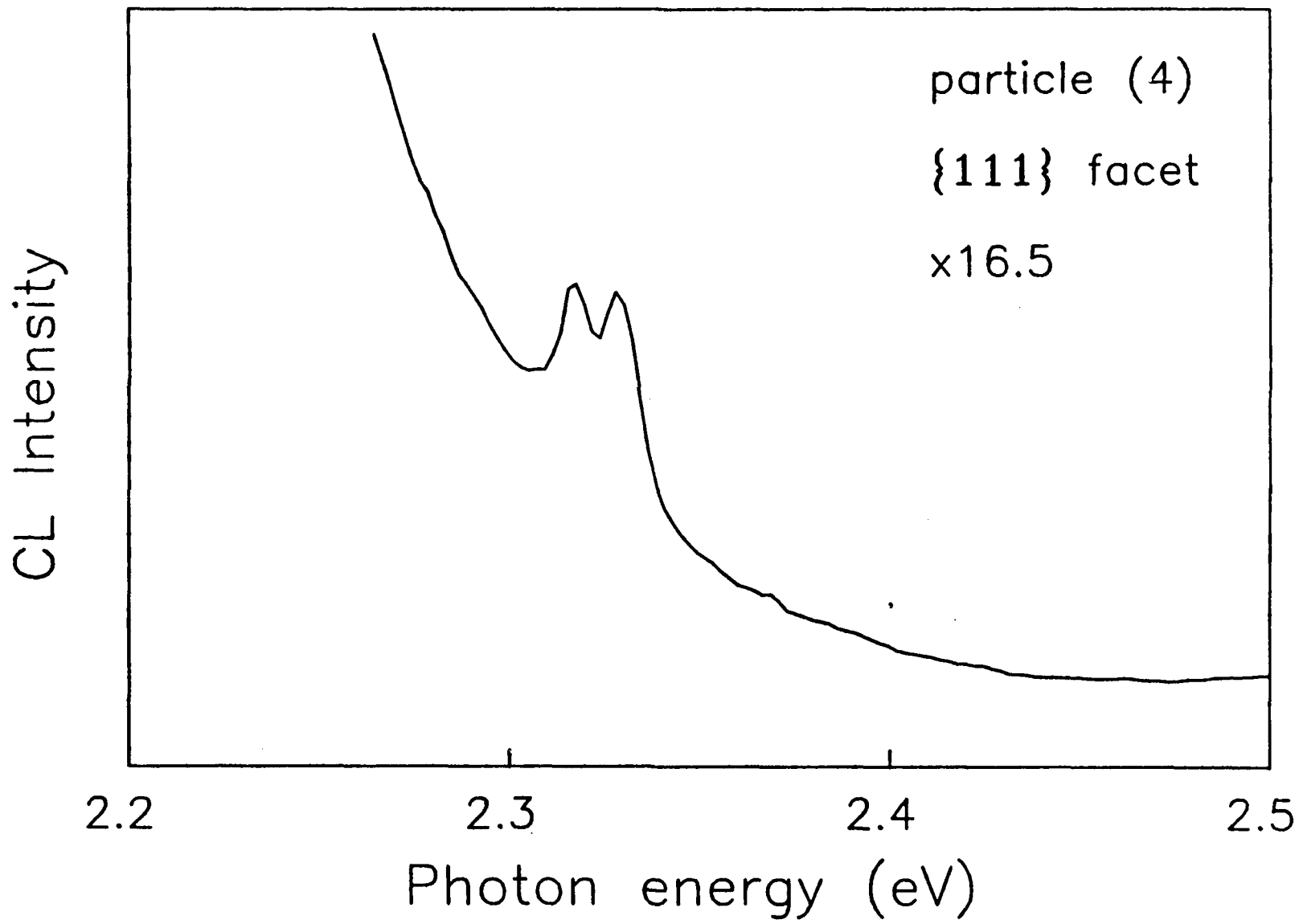
particle (4)
{111} facet
x16.5
CL Intensity
2.2
2.3
2.4
2.5
Photon energy (eV)

FIG 5

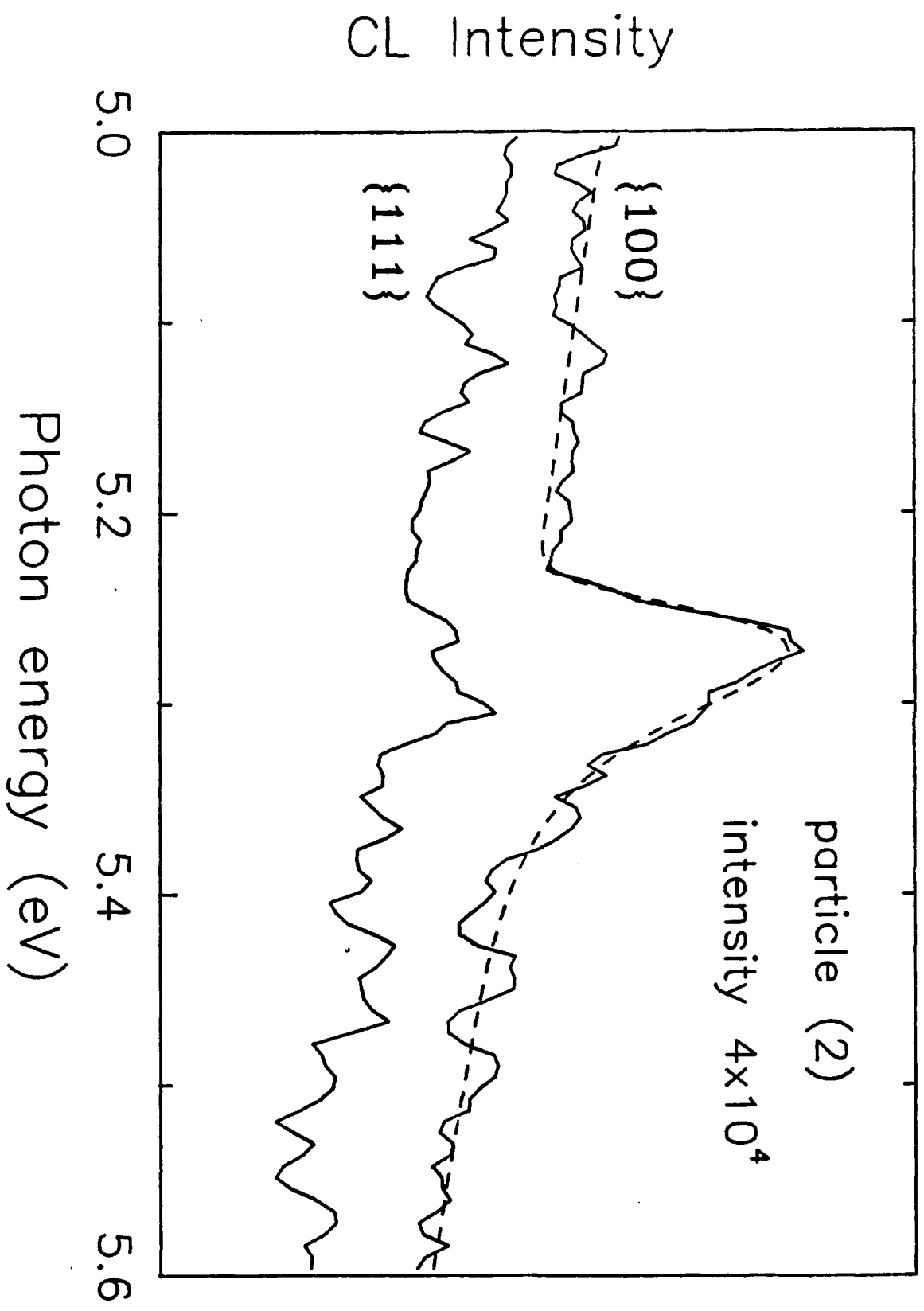
CL Intensity
{100}
{111}
particle (2)
intensity 4x10⁴
5.0
5.2
5.4
5.6
Photon energy (eV)

FIG 6

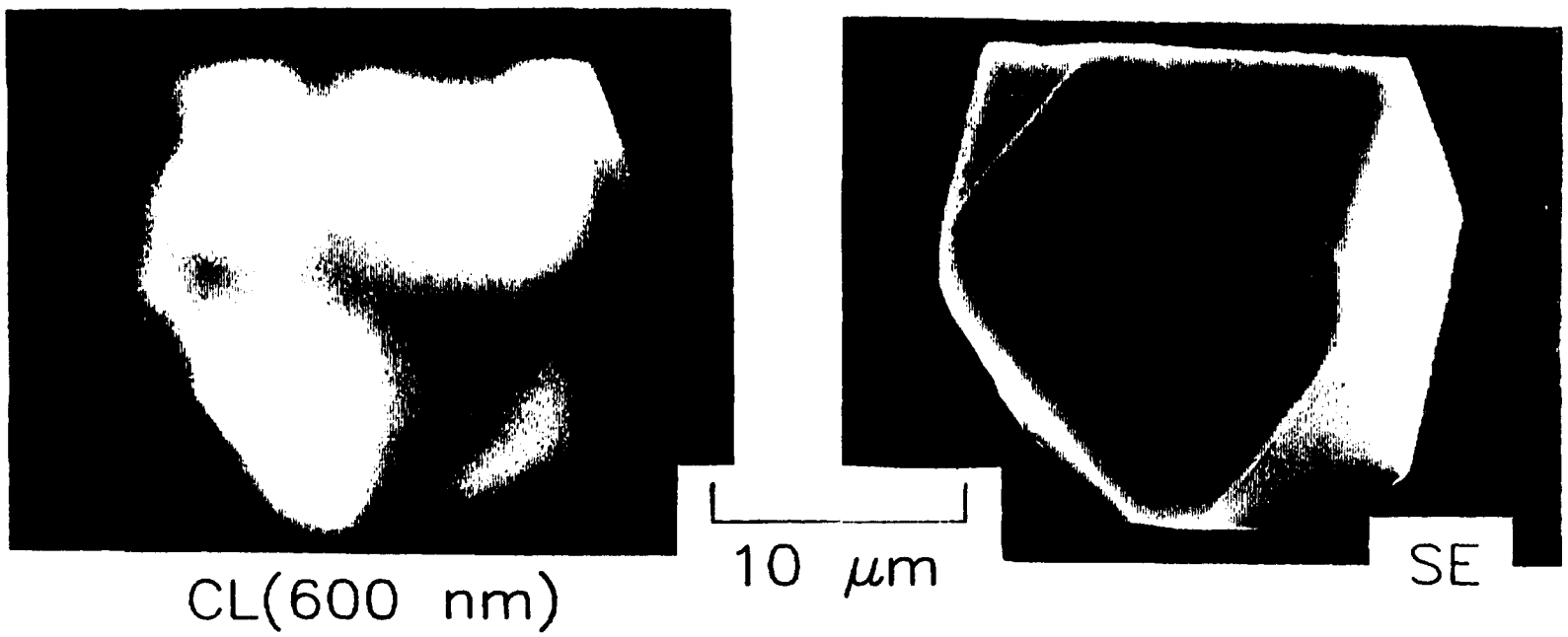

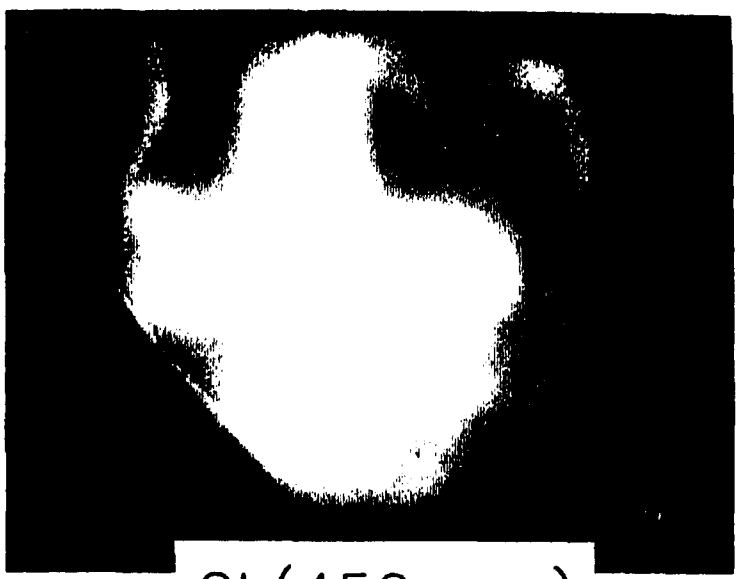

(a)

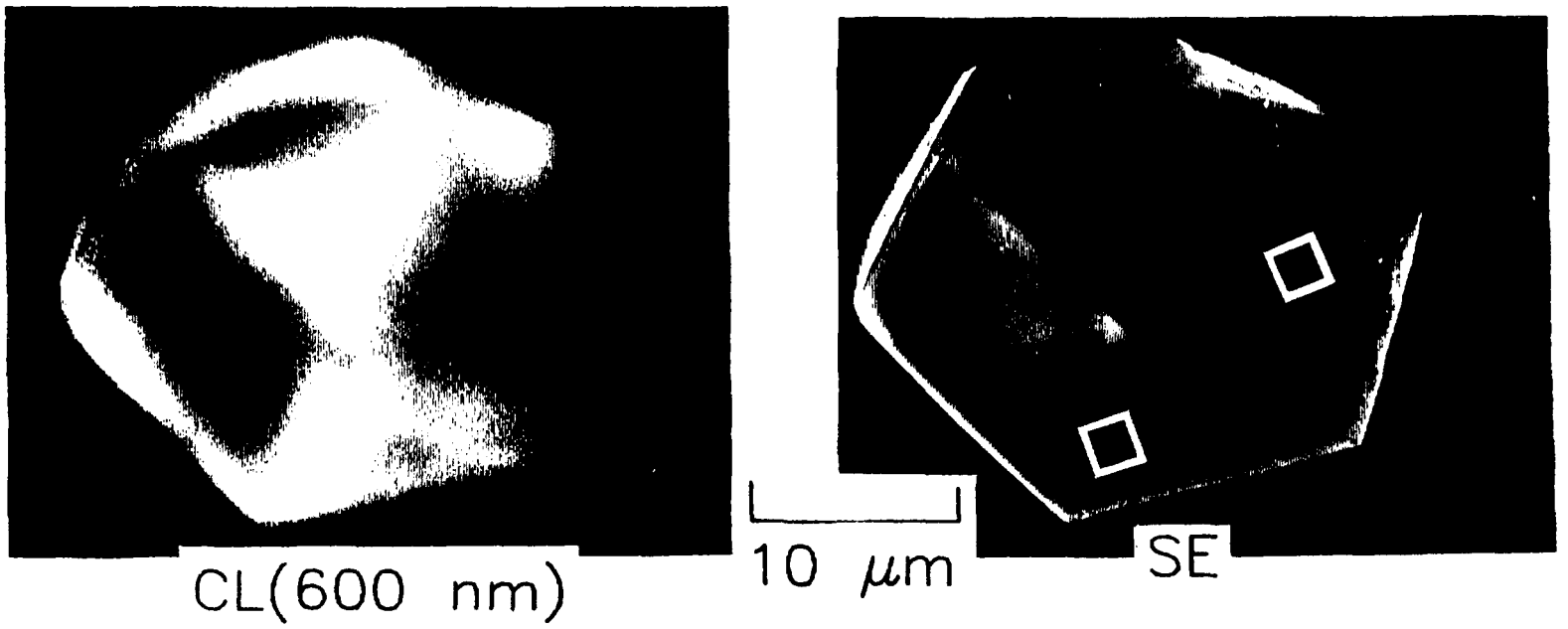

(b)

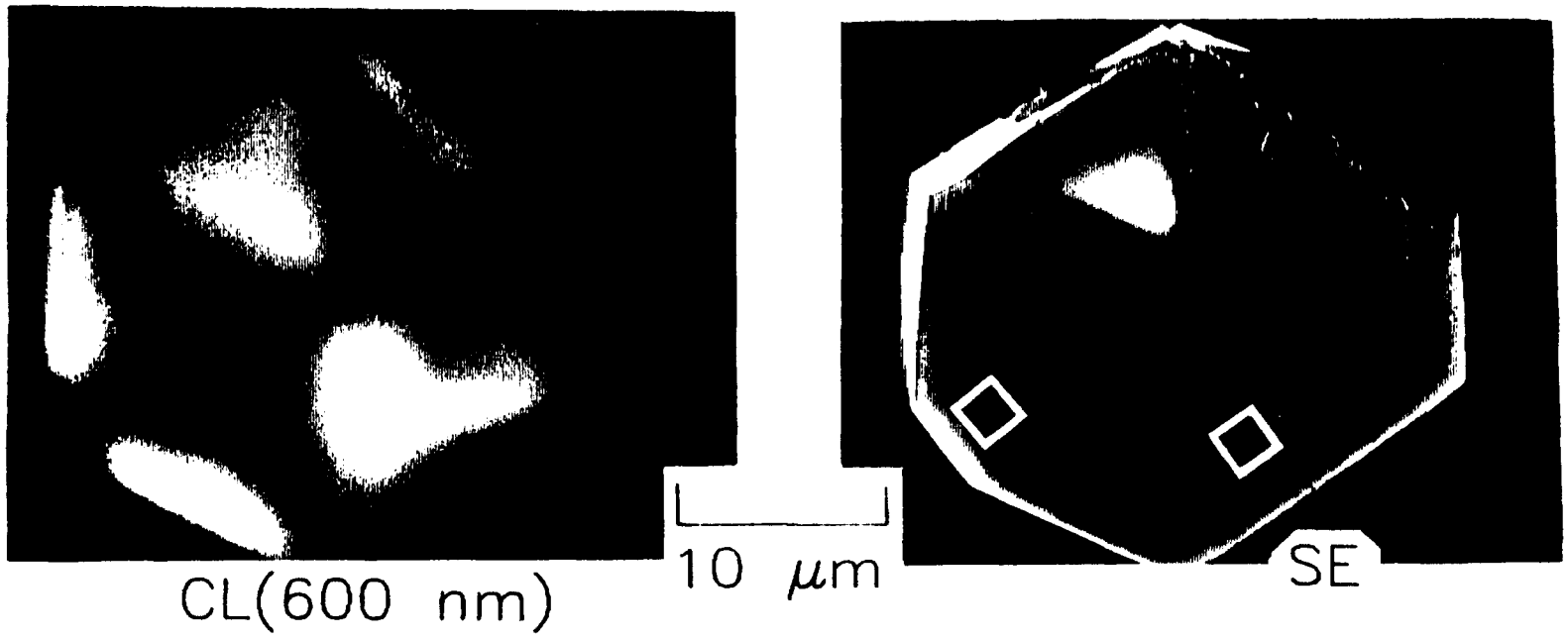

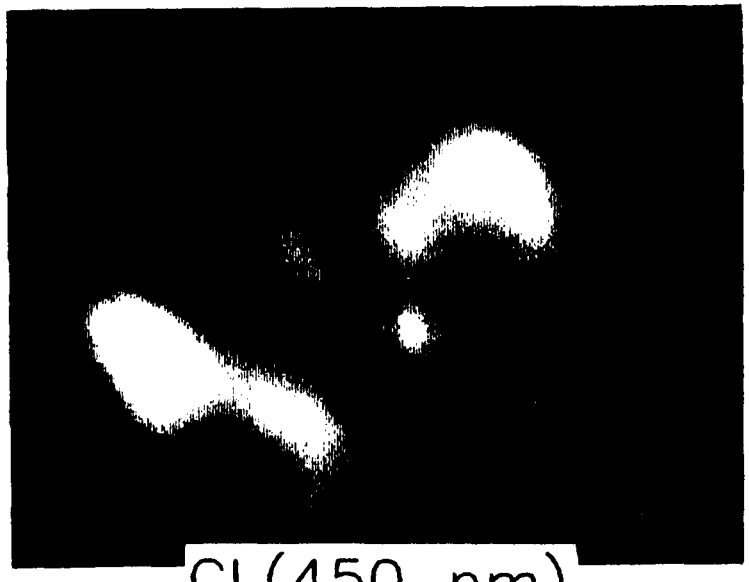

(c)

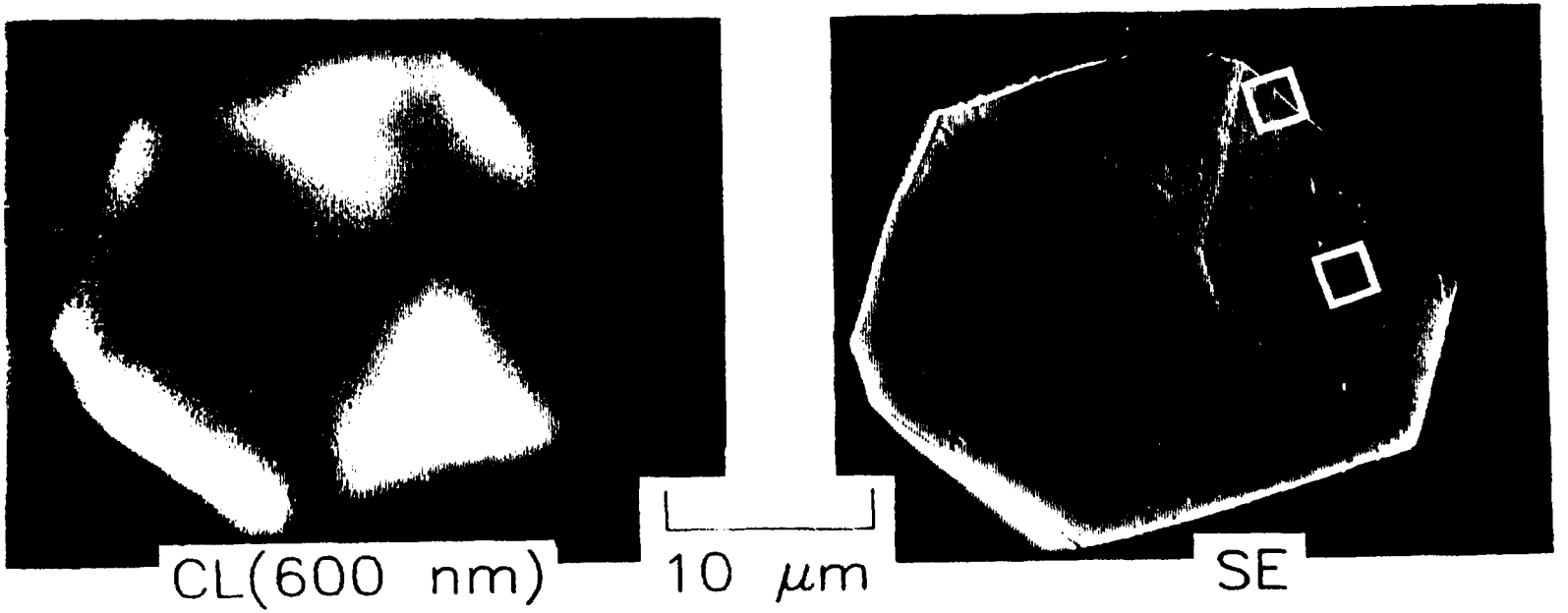

(d)

CL(600 nm)

10 μm

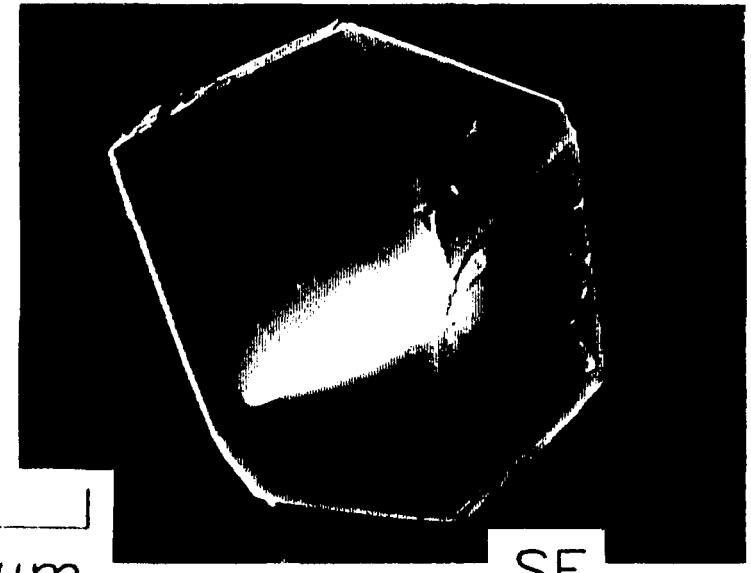

SE

CL(450 nm)

(e)

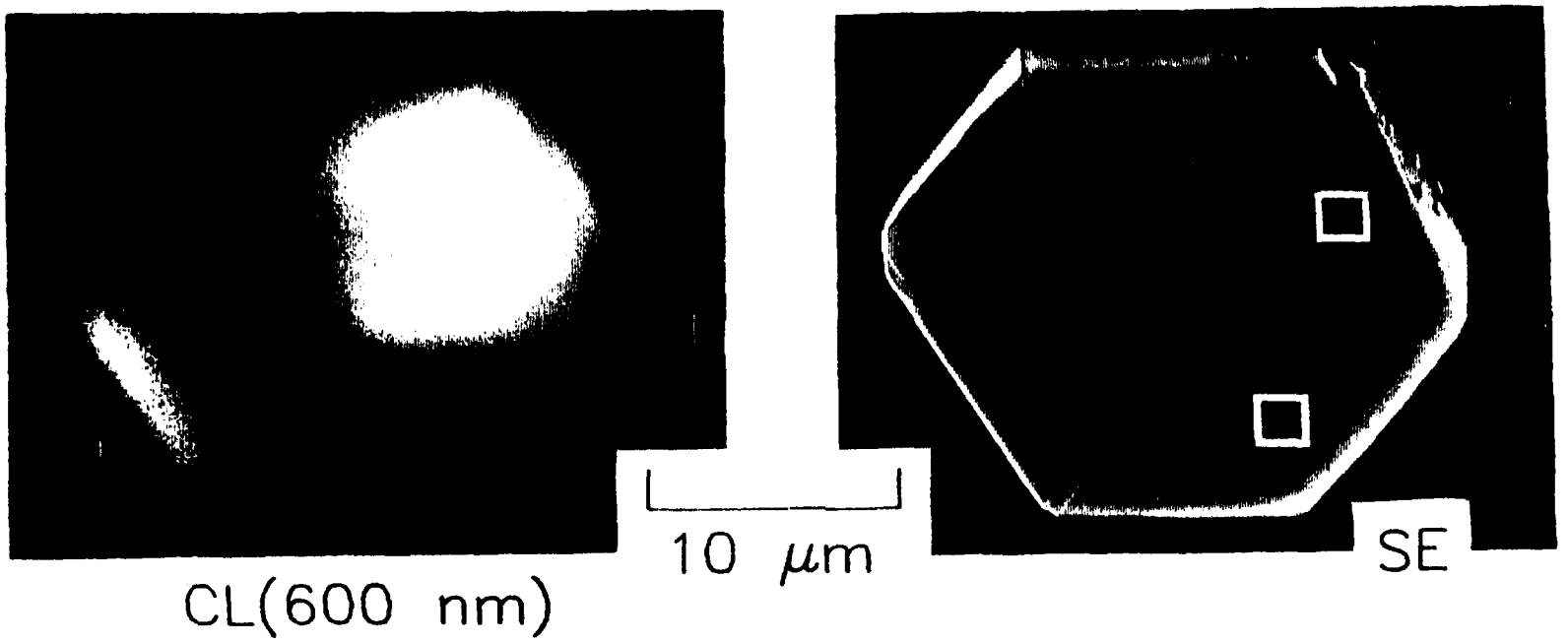

(f)

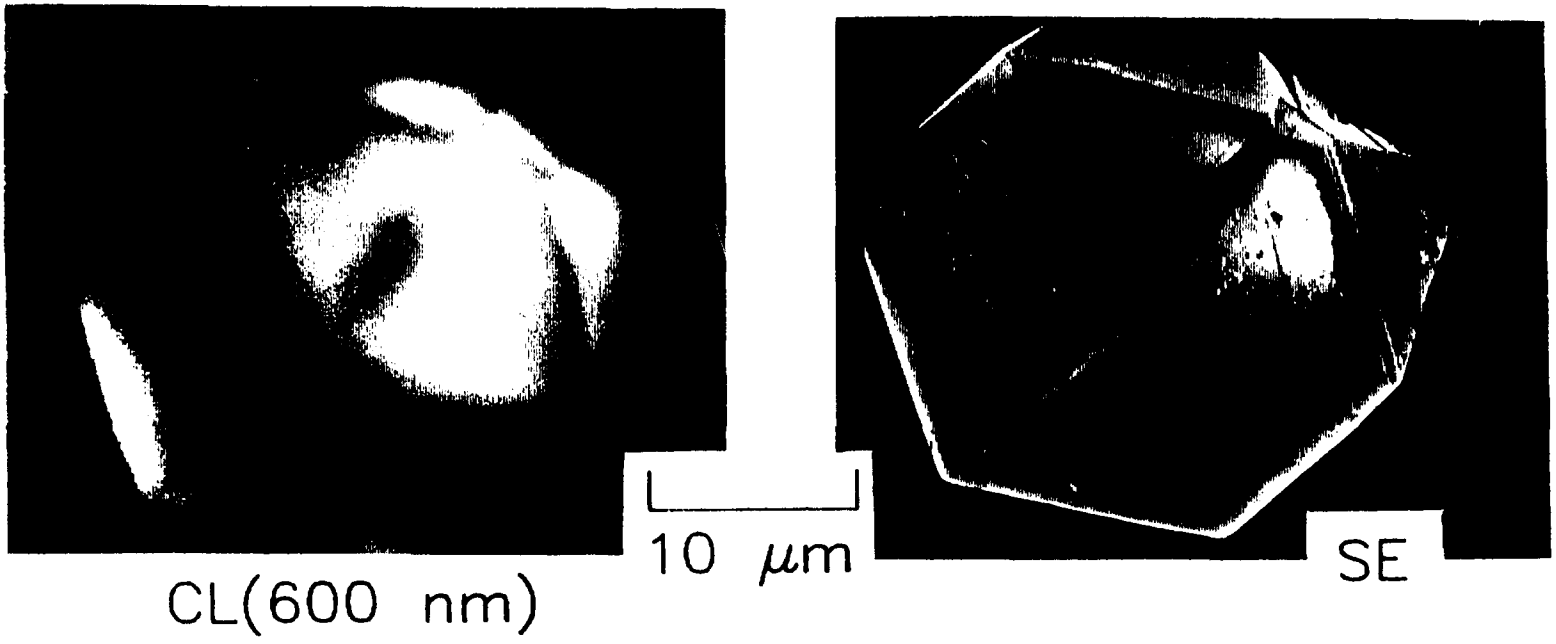

(g)

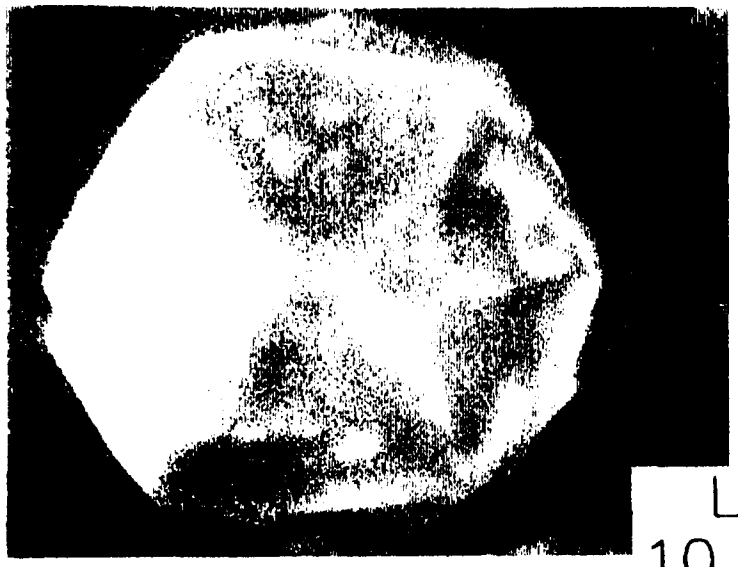

CL(600 nm)

10 μm

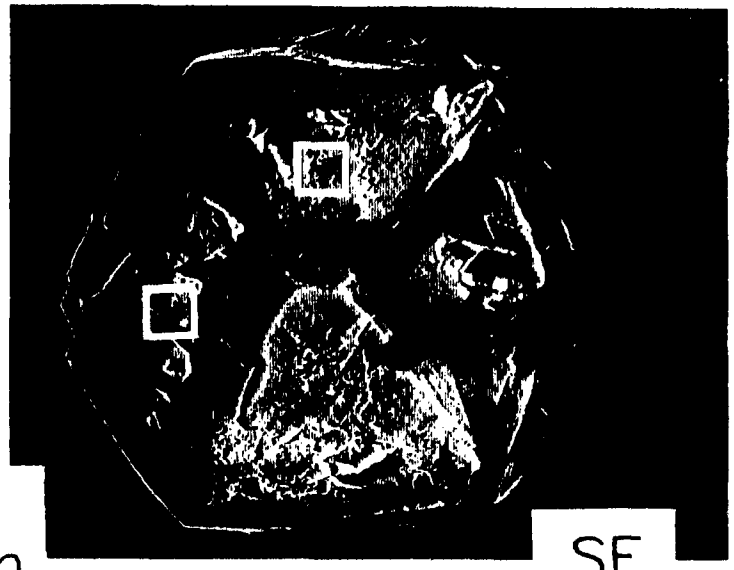

SE

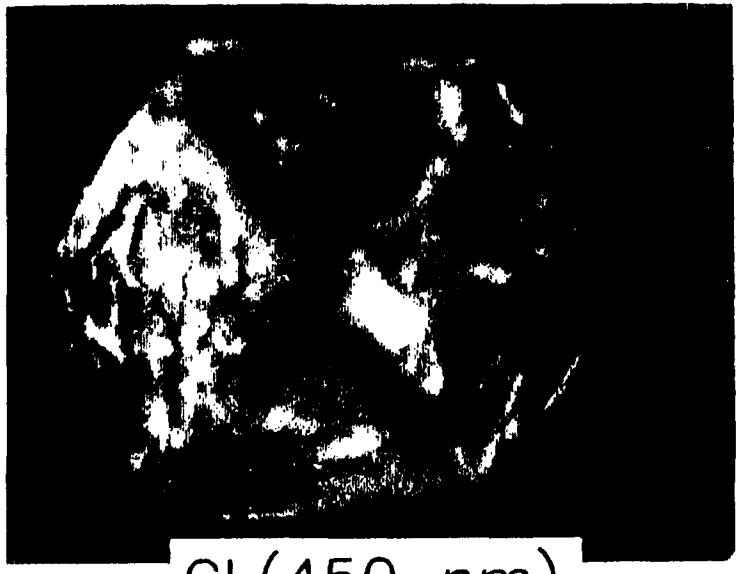

CL(450 nm)